

# Ballistic limit assessment for concrete slabs using the MHJC concrete model

M. Polanco-Loria

*SINTEF Materials and Chemistry, N-7465 Trondheim, Norway*

O.S. Hopperstad & T. Børvik

*Structural Impact Laboratory (SIMLab), Department of Structural Engineering, Norwegian University of Science and Technology (NTNU), N-7491 Trondheim, Norway*

**ABSTRACT:** A modified version of the Holmquist-Johnson-Cook (MHJC) model was developed by the authors to handle impact and penetration problems in concrete. In this modified version a new continuous pressure-shear function is adopted where the influence of the third deviatoric stress invariant is considered; in addition, a new strain-rate sensitivity formulation is included and finally three damage variables describing the tensile cracking, shear cracking and pore compaction mechanisms are introduced. Model parameters are obtained for two concrete qualities and perforation of concrete slabs by pointed projectiles is considered numerically and compared with experimental results from the literature. Ballistic limit assessments with deviations under 8 % when compared to the experiments are obtained.

## 1 INTRODUCTION

Concrete is a material of particular interest for the nuclear industry and fortification installations for defence purposes. Many important studies of the behaviour of concrete targets impacted by projectiles have been of an empirical nature and most of the experimental studies have focused on the determination of empirical formulae, Kennedy (1976), Bendor et al. (2005). On the other hand, the parallel development of numerical tools and new constitutive models for concrete has contributed to an increased use of numerical simulations for prediction of penetration and impact problems, Holmquist et al. (1983), Bourlion (1997), Riedel (1998). Different constitutive models for concrete are available for the analysis of concrete structures; however, the development of reliable and robust material laws for concrete subjected to high-intensity loading of short duration is subject of current research. Complex state of stress is generated in reinforced concrete structures impacted by free-flying projectiles. Under a multi-axial state of stress the damage mechanisms activated are highly dependent on the loading path imposed. For concrete materials under static loading conditions, Mazars (1984) showed that depending on the load path imposed, different damage mechanisms are activated: cracking, shearing (e.g. mode II cracking) and compaction. In particular, for impact and penetration problems these three mechanisms are always present, as indicated by Bourlion (1997).

This requires the development of material models capable to describe concrete behaviour under low and high confining pressures. A literature review of existing experimental data and constitutive models for concrete materials under impact loading conditions was undertaken, Polanco-Loria (2001), and it was concluded that the HJC concrete model, Holmquist et al. (1983), represented a good compromise between simplicity and accuracy for large-scale computations. Some improvements of the original HJC model were recommended and evaluated, Polanco-Loria (2002), which forms the basis of this modified version (MHJC) presented in this work.

## 2 THE MODIFIED HJC CONCRETE MODEL

### 2.1 Pressure dependence

In order to avoid the discontinuous description of the original model and circumvent the identification of the cohesion parameter, the MHJC model adopts a simple continuous function defined by

$$\sigma_{eq}^* = B \left[ P^* + T^*(1-D) \right]^N F(\dot{\varepsilon}_{eq}^*) R(\theta, e) \leq S_{\max} \quad (1)$$

This equation holds for  $P^* \geq -T^*(1-D)$  and vanishes for  $P^* < -T^*(1-D)$ . Next,  $\sigma_{eq}^* = \sigma_{eq}/f_c$  is the normalized equivalent stress,  $P^* = P/f_c$  is the normalized pressure and  $\dot{\varepsilon}_{eq}^* = \dot{\varepsilon}_{eq}/\dot{\varepsilon}_0$  is the normalized strain rate, where  $\dot{\varepsilon}_{eq}$  is the equivalent deviatoric strain rate.

The normalizing parameters are the quasi-static uniaxial compressive strength  $f_c$  and the reference strain rate  $\dot{\epsilon}_0$ . Further,  $B$  is the pressure hardening coefficient,  $N$  is the pressure hardening exponent,  $C$  is the strain rate sensitivity coefficient, and  $S_{\max}$  is the normalized maximum strength that can be developed. Material degradation is described by the damage variable  $D$ , resulting in reduction of the cohesive strength. In the negative pressure regime ( $P^* < 0$ ) the normalized hydrostatic tension  $T^* = T/f_c$  is introduced with  $T$  as the maximum hydrostatic tension the material can withstand. The new functions  $F(\dot{\epsilon}_{eq}^*)$  and  $R(\theta, e)$  are defined below.

By assuming  $1.8 \leq B \leq 2.0$  and  $0.60 \leq N \leq 0.80$  the MHJC material model agrees with experimental results for the compressive meridian, reported in the literature (Chen 1982), assuming an undamaged state as illustrated in Figure 1. In a complete damaged state ( $D=1$ ) concrete behaves as a granular material and the term  $T^*(1-D)$  in Equation 1 vanishes.

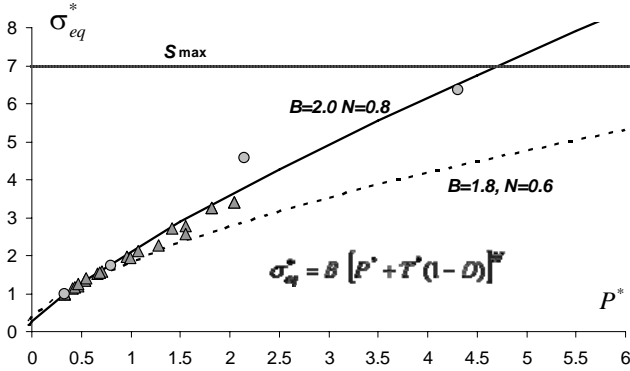


Figure 1 Undamaged compressive meridian strength response of the MHJC model.

## 2.2 Influence of the third shear stress invariant

Tri-axial experiments on concrete clearly demonstrate the substantial difference of shear strength between the compressive and tensile meridian, Chen (1982). A reduction of the shear strength on the compressive meridian can be considered by introducing a function  $R$  depending on the deviatoric polar angle  $\theta$  and the normalized out-of-roundness parameter  $e$ , as proposed by Willam & Warnke (1975), viz.

$$R(\theta, e) = \frac{2(1-e^2)\cos\theta + (2e-1)\left[4(1-e^2)\cos^2\theta + 5e^2 - 4e\right]^{1/2}}{4(1-e^2)\cos^2\theta + (1-2e)^2} \quad (2)$$

where  $\theta$  is defined as

$$\theta = \frac{1}{3} \cos^{-1} \left( \frac{27|S|}{2\sigma_{eq}^3} \right) \quad (3)$$

in which  $|S|$  is the determinant of the deviatoric stress tensor  $S$ . The parameter  $e$  is a shape factor that describes the out-of-roundness of the deviatoric trace. By adopting the Willam-Warnke concrete model, Chen (1982) found that the shape factor changes from 0.684 to 0.705 when the pressure goes from 0.33 to 2.33. For moderate pressure levels  $1 < P^* < 3$ , Launay & Gachon (1970) reported a shape factor around  $e = 0.7$ . Based on these observations, a linear dependency between the pressure and the shape factor was assumed. The reduction factor  $R(\theta, e)$  is introduced in a multiplicative way in Equation 1 as proposed by Riedel (1998).

## 2.3 Rate dependence

In the original HJC concrete model the strain rate influence  $F(\dot{\epsilon}^*)$  is defined as a linear function on a logarithmic scale of the strain rate and characterized by the slope  $C$ . However, in order to avoid negative values of  $F(\dot{\epsilon}^*)$  for relative strain rate values  $\dot{\epsilon}^* < 1$ , while keeping the two-parameter formulation, the following expression proposed by Camacho & Ortiz (1997) and largely used by Børvik et al. (1999) for metals is adopted, viz.

$$F(\dot{\epsilon}_{eq}^*) = \left[ 1 + \dot{\epsilon}_{eq}^* \right]^C \quad (4)$$

where the parameter  $C$  describes the non-linear character of the rate effect. Practically the relative increase in compression strength, found in the literature, (CEB 1988, Bischoff & Perry 1991), is always related to the static case which involves strain rate values of about  $10^{-5} s^{-1}$ . For this reason we assumed such a value as the reference strain rate  $\dot{\epsilon}_0$ .

## 2.4 Pressure-volume response

The pressure-compaction response is illustrated in Figure 2. The pressure  $P$  is defined as a function of the volumetric strain, as in the original paper of Holmquist et al. (1983)

$$\mu = \frac{\rho}{\rho_0} - 1 \quad (5)$$

where  $\rho_0$  and  $\rho$  are the initial and actual densities, respectively. In compression, the behaviour is divided into three regions. The first region is linear elastic and limited by  $(\mu_{crush}, P_{crush})$ . At this state the second region starts, which involves crushing of the concrete and production of plastic volumetric strains, and it continues until  $(\mu_{lock}, P_{lock})$ . The air voids are then assumed to be fully compressed out of the concrete (compaction damage). In the third region, the concrete is fully dense, i.e. all air voids are removed from the material.

The first and second regions are modelled by a classical incremental elasto-plastic-damaging formulation with a linear strain hardening and scalar damage

(compaction) assumptions, while the third region is modelled by assuming that concrete is completely elastic (crushed material with no tensile capacity).

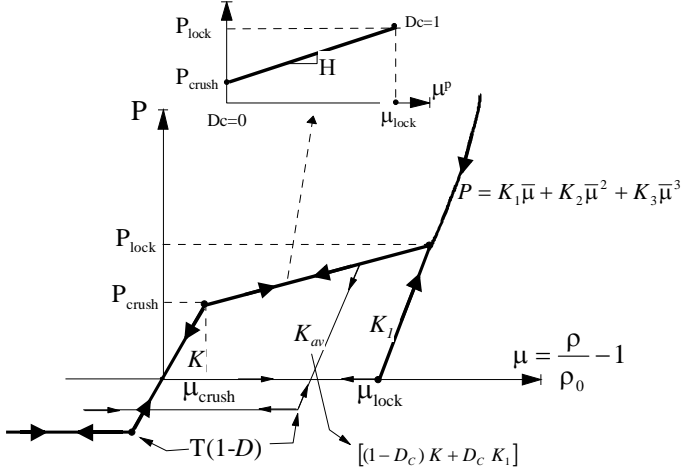


Figure 2. Pressure-volume response of the MHJC model

In particular, the total volumetric strain increment is separated into its elastic and plastic contributions, according to

$$\Delta\mu = \Delta\mu^e + \Delta\mu^p \quad (6)$$

The volumetric strain hardening modulus  $H$ , see Figure 2, is defined by

$$H = \frac{P_{lock} - P_{crush}}{\mu_{lock}} \quad (7)$$

The volumetric plastic strain increment  $\Delta\mu^p$  is found with a classical elastic predictor-plastic corrector procedure. For this a trial pressure  $P_{trial}$  is calculated assuming an elastic behaviour as

$$P_{trial} = K_{av}\mu \quad (8)$$

where the averaged elastic bulk modulus  $K_{av}$  is defined according to the compaction damage value ( $D_c$ , to be defined later) as

$$K_{av} = (1 - D_c)K + D_c K_1 \quad (9)$$

By comparing the pressure in the previous step and the trial calculation one can deduce the incremental volumetric plastic strains according to

$$\Delta\mu^p = \begin{cases} 0 & \text{if } P_{trial} \leq P_{i-1} \\ \frac{P_{trial} - P_{i-1}}{(K_{av} + H)} & \text{if } P_{trial} > P_{i-1} \end{cases} \quad (10)$$

Finally, an updating of the plastic volumetric strain and pressure is required. The pressure-volume behaviour in the fully compacted region ( $P > P_{lock}$ ) follows a non-linear elastic behaviour. For this a modified volumetric strain is introduced

$$\bar{\mu} = \frac{\mu - \mu_{lock}}{1 + \mu_{lock}} = \frac{\rho_{grain}}{\rho_0} - 1 \quad (11)$$

where  $\rho_{grain}$  is the grain density and it shows that  $\bar{\mu}$  represents the volumetric strain of the grain material. This material follows a non-linear elastic behaviour of type

$$P = K_1 \bar{\mu} + K_2 \bar{\mu}^2 + K_3 \bar{\mu}^3 \quad (12)$$

This equation is used as long as  $D_c = 1$  (fully compacted material). The modified volumetric strain  $\bar{\mu}$  is used in the constitutive relation so that the constants  $K_1, K_2$  and  $K_3$  are equivalent to those for a material without voids. Because no volumetric plastic strains can be generated for tensile (negative) pressures, the elastic predictor scheme works also in this regime by updating the pressure according to

$$P_i = \max(K_{av}\mu_i^e, -T(1-D)) \quad (13)$$

It is interesting to observe that in the fully compacted zone  $D = D_c = 1$ , the tensile threshold vanishes.

## 2.5 Damage behaviour

The main idea in this work is to treat the three basic damage mechanisms separately, and for this purpose three internal damage variables  $D_T$ ,  $D_S$  and  $D_C$ , representing the tensile, shear and compaction damage, respectively, are introduced.

### 2.5.1 Tensile damage (brittle cracking)

Prediction of tensile cracking has been largely studied and basically three types of models are commonly used: discrete, smeared and damage models. In these models the introduction of a crack formation criterion is required. By simplicity, it was decided here to use the hydrostatic tensile strain as the main indicator for crack formation. For this, the minimum value of the volumetric strain  $\mu$  (in the tensile regime) attained during the loading history is assumed as the equivalent strain for crack formation and it reads

$$\varepsilon_T^t = \min(\varepsilon_T^{t-1}, \min(0, \mu^t)) \quad (14)$$

where the superscripts  $t$  and  $t-1$  indicate the actual and previous increment, respectively. The tensile damage criterion is simply defined by

$$D_T = \begin{cases} 0 & \text{for } \varepsilon_T^t > \varepsilon_0 \\ 1 & \text{for } \varepsilon_T^t \leq \varepsilon_0 \end{cases} \quad (15)$$

where  $\varepsilon_0 = -\frac{f_t}{K}$  is the volumetric tensile strain threshold for crack formation.

### 2.5.2 Shear damage

The cumulative damage development proposed in the HJC original model, Holmquist et al. (1983), is adopted here. However, damage from shear and volumetric straining is separated. The evolution of the shear damage variable  $D_S$  is defined by

$$\Delta D_s = \frac{\Delta \varepsilon_{eq}^p}{\varepsilon_p^f} \quad (16)$$

The plastic strain to fracture  $\varepsilon_p^f$  is here adopted as in the original model in the form

$$\varepsilon_p^f = \alpha \left[ P^* + T^* \right]^\beta \geq (\varepsilon_p^f)_{\text{MIN}} \quad (17)$$

where  $\alpha$  and  $\beta$  are constants. The third damage constant  $(\varepsilon_p^f)_{\text{MIN}}$  is introduced to allow for a finite amount of plastic strain to fracture the material.

### 2.5.3 Compaction damage

Damage compaction due to plastic volumetric strain is defined by the pressure-volume law. For this mechanism the cohesive strength of the concrete is lost during air voids collapse (i.e. the pore compaction contributes to damage) and the bulk stiffness increases (i.e. the bulk modulus approaches to that of a compacted material). Thus, an internal compaction damage variable  $D_C$  can be defined as

$$\Delta D_C = \frac{\Delta \mu^p}{\mu_{lock}} \quad (18)$$

Here,  $\Delta \mu^p$  is the incremental plastic volumetric strain (see Equation 10) and  $\mu_{lock}$  is the plastic volumetric strain of the fully compacted granular material (an input parameter).

### 2.5.4 Total damage

The combination of three different damage mechanisms, defined by the damage variables  $D_T$ ,  $D_s$  and  $D_C$ , into one representative scalar value  $D$  is questionable. Under the framework of the scalar damage theory we decide to exclude  $D_T$  in the averaging proposal based on the argument that tensile cracking effect is reduced by the presence of the steel reinforcement (if present) and the competition between crack closure and opening caused by the compressive and tensile waves propagation. Thus, the damage variable  $D_T$  is used only as a tensile damage indicator (is used only for post-processing purposes). We consider  $D_s$  and  $D_C$  in the averaging procedure where the total damage effect is calculated according

$$(1-D) = \sqrt{(1-D_s)(1-D_C)} \quad (19)$$

A similar averaging procedure was proposed by Riedel (1998). A complete description of the MHJC concrete model can be found in Polanco-Loria et al. (2006).

## 3 PARAMETERS IDENTIFICATION

At first, a complete calibration of the parameters involved in MHJC seems complex and expensive because the identification of 19 parameters required.

However, this task can be simplified if one considers a reduced number of tests complemented with inverse modelling and assumptions related to some values. For instance, the material strength characterization requires the uniaxial compressive strength  $f_c$  and the initial density  $\rho_0$ , while the uniaxial tensile strength  $f_t$  can be related to the compressive strength, i.e.  $f_t = 0.54\sqrt{f_c}$ , according to the FIB/CEB (1990). Also the Young's modulus  $E$  can be related to the compressive strength, i.e.  $E = 11700(f_c)^{0.3}$  (Sellevold et al. 1994). A Poisson's ratio of  $\nu = 0.2$  can be assumed. The shear-pressure behaviour can be represented by assuming values of  $1.8 \leq B \leq 2.0$  and  $0.60 \leq N \leq 0.80$ , see section 2.1. It should be pointed out that "special" concretes can deviate largely from the  $B$  and  $N$  values previously proposed. As a matter of fact, in the experimental program on perforation of concrete slabs, conducted by Hanchak et al. (1992), two concrete qualities C\_48 and C\_140 with special glassy gravel (called Steilacoon Glacial) were used. The hardness of this type of gravel is slightly lower than a quartz mineral type. The shear-pressure response of a series of triaxial tests reported by Hanchak et al. (1992) is illustrated in Figure 3. By a fitting procedure one finds values of  $B = 1.4$ ,  $N = 0.65$  and  $B = 1.30$ ,  $N = 0.45$  for the concrete qualities of C\_48 and C\_140, respectively. To sum up, two triaxial compression tests (in addition to the uniaxial compression) would be preferable for accurate identification of  $B$  and  $N$ .

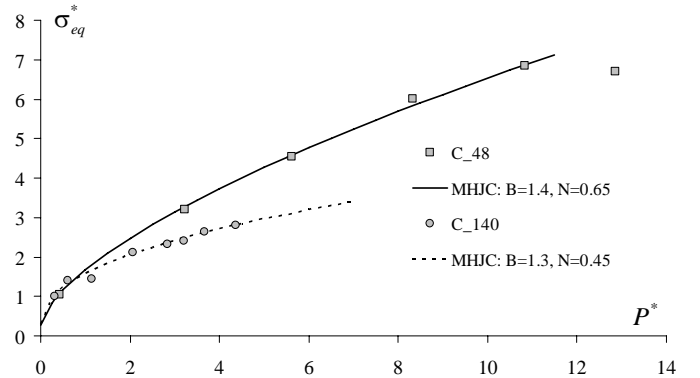


Figure 3. Shear-pressure response. Identification of  $B$  and  $N$

Next, some of the parameters involved in the pressure-volume law can easily be identified. For instance, from elasticity  $P_{crush} = f_c/3$  and  $\mu_{crush} = f_c(1-2\nu)/E$ , while  $\mu_{lock}$  can be assessed from the density of the gravel material ( $\rho_{grain}$ ) and the initial density of concrete ( $\rho_0$ ) using  $\mu_{lock} = \rho_{grain}/\rho_0 - 1$ . Unfortunately, the identification of  $P_{lock}$  and  $(K_1, K_2, K_3)$  requires hydrostatic tests at very high pressure levels. Based on common results from the literature  $P_{lock} \geq 600$  MPa  $K_1 = 8500$  MPa  $K_2 = -17100$  MPa and  $K_3 = 20800$  MPa are representative values for concrete materials (Holmquist et al. 1983, Johnson et al. 1998). In order to avoid the identification of ductility diagrams (fracture strain

versus triaxiality), values of  $\alpha = 0.04$  and  $\beta = 1.0$  can be assumed to represent the concrete damage behaviour with reasonable accuracy (Holmquist et al. 1983, Johnson et al. 1998). The fracture parameter  $(\varepsilon_p^f)_{\text{MIN}}$  with values of 0.01 (low strength quality) and 0.005 (high strength quality) can be introduced to represent different embrittlement characteristics. Finally, for penetration problems the rate sensitivity parameter  $C$  can be identified by inverse modelling in the high impact velocity region (i.e. from 500 to 1000 m/s). With this procedure values of  $C = 0.04$  (C\_48) and  $C = 0.025$  (C\_140) were found. These findings further corroborate the experimental observations that high strength concretes are less sensitive to variation in strain rates (CEB 1988, Bischoff & Perry 1991).

#### 4 NUMERICAL SIMULATION OF PERFORATION OF CONCRETE SLABS

##### 4.1 *Experimental study of Hanchak et al.*

The ballistic limit computations are based on the test performed by Hanchak et al. (1992), where square reinforced concrete plates of  $610 \times 610 \times 178 \text{ mm}^3$  were tested. Three layers of square-pattern reinforcement steel rods with a diameter of 5.6 mm were used. Two concrete qualities C\_48 and C140 with uniaxial compressive strength of  $f_c = 48$  and 140 MPa and uniaxial tensile strength of  $f_t = 4$  and 5 MPa were reported. In addition to the pressure-compaction curves, triaxial tests were performed under various confining pressure levels such that shear strength versus pressure curves could be established, see Figure 3. A 30-mm, smooth-bore powder gun was used to launch 0.50 kg ogival-nose steel projectiles with a length of 143.7 mm and a diameter of 25.4 mm. In the tests, initial and residual projectile velocities were measured. These values were used to construct initial versus residual velocity curves for the two concrete qualities and from these diagrams ballistic limits were deduced. Hanchak et al.'s main conclusion was that even though the unconfined compressive strength was increased by a factor of three, the ballistic limit velocity only increased by 20%.

##### 4.2 *Concrete slabs with $f_c = 48$ MPa*

The MHJC concrete model was implemented in LS-DYNA (1999) and finite element analyses with 2D axisymmetric elements were used in the simulations. A reduced integration scheme with hourglass control was adopted. For the concrete slab a total of 100 elements were used through the thickness and 50 elements along the radius. The steel reinforcement was not included in the simulations since its effect on the perforation resistance was found negligible (Holmquist et al. 1983). The set of input parameters as-

sumed are deduced from the recommendations of section 3. The steel projectile was modelled using a von Mises material model (Mat\_003 in LS-DYNA) with linear isotropic hardening. The main data used for the projectile included:  $E = 200 \text{ GPa}$ ,  $\nu = 0.3$ ,  $\sigma_Y = 1.72 \text{ GPa}$  and  $E_T = 15 \text{ GPa}$  (tangent modulus). No strain rate effect was considered. The original density of the projectile ( $8020 \text{ Kg/m}^3$ ) was slightly modified to  $8300 \text{ Kg/m}^3$  to obtain the total launch package mass of 0.53 Kg. In the present calculations, we adopted the element erosion option of LS-DYNA with a criterion based on the maximal principal strain with a failure strain value of  $(\varepsilon_1)_{\text{MAX}} = 1.0$  (based on similar values used in Holmquist et al. 1983). The 2D\_automatic\_single\_surface contact option of LS-DYNA was used to define the contact behaviour between steel and concrete without friction. The rate sensitivity parameter value of  $C = 0.04$  was used based on the residual velocity predictions of the previous section 3. The numerical predictions of the residual velocity are compared with the experimental findings (Hanchak et al. 1992) for the C\_48 concrete in Figure 4. The MHJC compares very well with the experimental values, in particular for impact velocities higher than 400 m/s. The predicted ballistic limit (325 m/s) deviates by less than 5% from the experimental value (340 m/s). The tensile damage (cracking) evolution during the perforation process is illustrated in Figure 5.

##### 4.3 *Concrete slabs with $f_c = 140$ MPa*

The uniaxial compressive and tensile strength of this concrete was  $f_c = 140 \text{ MPa}$  and  $f_t = 5 \text{ MPa}$ , respectively. A new set of input parameters based on the recommendations of section 3 is used. We used the material data of the previous example for the projectile. The element erosion option with a failure strain value of  $(\varepsilon_1)_{\text{MAX}} = 1.0$  and the 2D\_automatic\_single\_surface contact option without friction of LS-DYNA were once again adopted. A rate sensitivity parameter value of  $C = 0.025$  was used for this case (see section 3). In addition, the plastic fracture strain limit is reduced to  $(\varepsilon_p^f)_{\text{MIN}} = 0.004$  in order to account for the brittle nature of high strength concrete. The numerical predictions of residual velocity are compared with the experimental findings as shown in Figure 4. Also in this case the MHJC compares well with the experiments, and the predicted ballistic limit (370 m/s) deviates by less than 8% from the experimental one (400 m/s).

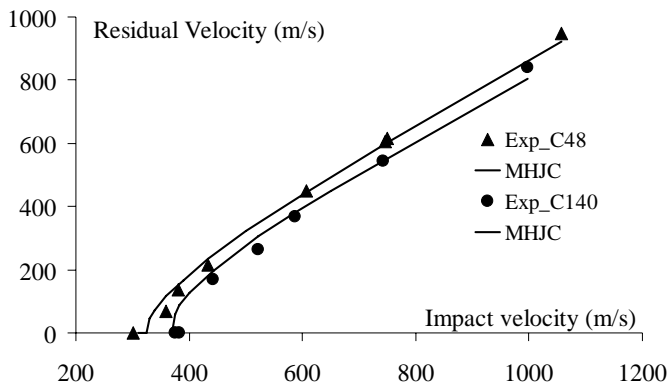


Figure 4. Ballistic limit predictions using the MHJC

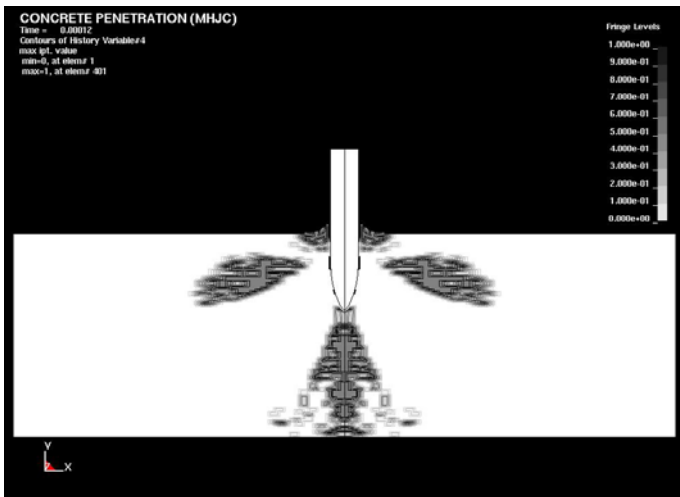


Figure 5. Tensile damage development during concrete perforation after 0.12 ms

## 5 CONCLUSIONS

A modified version of HJC model for concrete materials subjected to impact loading has been investigated. In this modified version a new continuous pressure-shear function is adopted where the influence of the third deviatoric stress invariant is considered; in addition, a new strain-rate sensitivity formulation is included and finally three damage variables describing the tensile cracking, shear cracking and pore compaction mechanisms are introduced. A proposal for parameter identification is provided. Ballistic limit assessments with deviations under 8%, when compared to experimental results from the literature, were found, indicating that the MHJC model represents a good compromise between simplicity and accuracy for large scale-computations of concrete plates impacted by projectiles.

## REFERENCES

Ben-Dor, G., Dubinsky, A. & Elperin, T. 2005. Ballistic Impact: Recent advances in analytical modeling of plate penetration dynamics-A review. *Applied Mechanics Reviews*, 58: 355-371.

- Bischoff, P.H. & Perry, S.H. 1991. Compressive behaviour of concrete at high strain rates. *Materials and Structures, RILEM*, 24: 425-450.
- Burlion, N. 1997. *Compaction des betons: elements de modelisation et caracterisation experimentale*. Ph.D. Dissertation, LMT, ENS de Cachan, France.
- Børvik, T., Langseth, M., Hopperstad, O.S. & Malo, K.A. 1999. Ballistic penetration of steel plates. *International Journal of Impact Engineering*, 18 (2): 855-886.
- Camacho G.T. & Ortiz M. 1997. Adaptive Lagrangian modelling of ballistic penetration of metallic targets. *Computer Methods in Applied Mechanics and Engineering*, 142: 269-301.
- CEB 1988. *Concrete structures under impact and impulsive loading*. CEB bulletin d'information No. 187, Lausanne, Switzerland.
- Chen, W.F. 1982. *Plasticity in reinforced concrete*. Mc Graw Hill, New York.
- FIB/CEB 1990. *State of the art report: High strength concrete Switzerland*.
- Hanchak, S.J., Forrestal, M.J., Young, E.R. and Ehrigott, J.Q. 1992. Perforation of concrete slabs with 48 MPa and 140 MPa unconfined compressive strengths. *International Journal of Impact Engineering*, 12 (1): 1-7.
- Holmquist, T.J., Johnson, G.R. and Cook, W.H. 1993. A computational constitutive model for concrete subjected to large strains, high strain rates and high pressures. *Proceedings of 14th International Symposium on Ballistics, Canada*.
- Johnson, G.R. Beissel, S.R., Holmquist, T.J. & Frew, D.J. 1998. Computer radial stresses in a concrete target penetrated by a steel projectile. *Proceedings of 5<sup>th</sup> International Conference on Structures under Shock and Impact V*. Computational Mechanics Publications: 793-806.
- Kennedy, R.P. 1976. A review of procedures for the analysis and design of concrete structures to resist missile impact effects. *Nuclear Engineering and Design*, 37: 183-203.
- Launey, P. & Gachon H. 1970. A study of the failure of concrete under combined compressive stress. *University of Illinois, Engineering Experimental Station, Bulletin No. 185*. USA.
- LS-DYNA. 1999. *Keyword User's Manual*. Ver. 950, Livermore Software Technology Corporation, LSCT.
- Mazars, J. 1984. *Application de la mecanique de l'endommagement au comportement nonlineaire et la rupture du beton de structure*. These de Doctorate d'Etat, LMT, Universite de Paris, France.
- Polanco-Loria, M. 2001. *Constitutive models for concrete materials under impact loading conditions*. SINTEF report STF24 F00315, Trondheim, Norway.
- Polanco-Loria, M. 2002. *Improvements to the HJC concrete model in LS-DYNA*. SINTEF report STF24 F01286, Trondheim, Norway.
- Polanco-Loria, M., Hopperstad, O.S., Børvik, T. & Berstad, T. 2006. *Numerical predictions of ballistic limits for concrete slabs using a modified version of the HJC concrete model*. Submitted for publication to the *International Journal of Impact Engineering*.
- Riedel, W. 1998. *Ein makroskopisches, modulares Betonmodell für Hydrocodes mit Verfestigung, Scädigung, Entfestigung, Drei-Ivariantenabhängigkeit und Kappe*, Bericht 7/98, Fraunhofer Institut für Kurzezeitdynamik-Ernst-Mach-Institut, Freiburg i. Br.
- Sellevoid, E., Justnes, H, Smepllass, S. & Hansen, E.A. 1994. *Selected properties of high performance concrete*. Advances in Cement and Concrete, Ed. Grutzeck and Sarkar, New England: 562-609.
- Willam, K.J. & Warnke, E.P. 1975. *Constitutive model for the triaxial behaviour of concrete*. Seminar on concrete structures subjected to triaxial stresses, IABSE Proc. 19, Italy.